# A general non-Fourier Stefan problem formulation that accounts for memory effects

Vaughan R. Voller[1] and Sabrina Roscani[2,3]

[1]Department of Civil, Environmental and Geo- Engineering, University of Minnesota, Minneapolis, Mn 55455, USA. *E-mail:* volle001@umn.edu

[2]Depto. Matemática, FCE, Universidad Austral, Paraguay 1950, S2000FZF Rosario, Argentina.

[3]CONICET, Godoy Cruz 2290, Buenos Aires C1425FQB, Argentina. *E-mail:* sabrinaroscani@gmail.com

**Abstract**

The Stefan problem is the classical model of a melting phase change. In heterogeneous systems, such phase changes can exhibit non-Fourier (anomalous) behaviors, where the advance of the melt interface does not follow the expected time scaling. These situations can be modeled by replacing the derivatives, in the governing partial differential equations, with fractional order derivatives. In particular, replacing the time derivatives leads to non-Fourier models that account for memory effects in the system. In this work, by using appropriate time convolution integrals, a general thermodynamic balance statement for melting phase problems, explicitly accounting for memory effects, is developed. From this balance, a general model formulation applicable to problems involving melting over a temperature range (i.e., a mushy region) is derived. A key component in this model is the representation of memory effects through the use of fractional derivative based constitutive models of the enthalpy and heat flux. On shrinking the mushy region to a single isotherm, a general sharp interface melting model is obtained. Here, in contrast to the classic Stefan problem, the fractional derivatives induce a natural regularization, such that the constitutive models for enthalpy and heat flux are continuous at the melt interface; a result confirmed through numerical simulation. To further support the theoretical findings, a physical example of a non-Fourier Stefan problem is presented. Overall the development and results in this paper underscore the importance of explicitly relating the development of fractional calculus models to the appropriate thermodynamic balance statements.

Keywords: Stefan Problem, Memory Effect, Fractional Derivative, Sharp Interface, Enthalpy Method

# 1 Introduction

Phase change problems are ubiquitous in the thermal sciences and of significant interest in both engineering [1–7] and mathematical [8–13] disciplines. The canonical phase change problem is the Stefan problem, describing the melting of pure ice [14]. The core feature in this problem is a sharp moving phase front (interface), separating the melt water from the ice. Typically, in studying the Stefan problem, the heat flux is modeled as a Fourier heat conduction, leading to solutions, in one-dimensional settings, where the melt front advances as the square root of time [8]. Currently, however, there is developing and active research focused on the study of so called non-Fourier Stefan problems [15–25]. Here, due to 'fast-paths' or 'memory' in the transport system, the length-time scaling can deviate from the expected square-root in time behavior. Possible models of this behavior can be built by using fractional calculus constructs, consisting of non-integer order integrals and derivatives [26–28]. In general, as summarized in [29–31], replacing the first order integer space derivative (the gradient) in the Fourier heat conduction equation, with a derivative of order $0 < \beta \leq 1$, produces so-called super-diffusive behavior—indicative of fast-paths—where the length-time scaling has an exponent $0.5 < \frac{\beta+1}{2} \leq 1$. In contrast, replacing the first order time derivative with a fractional order $0 < \alpha \leq 1$ accounts for 'memory' in the system, leading to a sub-diffusive exponent $0 < \frac{\alpha}{2} \leq 0.5$.

A general exploration of non-Fourier heat transport is provided in the review by Voller [32], this includes discussions on the mechanisms that may lead to non-Fourier behavior and examples of physical systems that exhibit this behavior. There is an extensive literature on non-Fourier problems associated with the freezing of biological tissue, an inherently heterogeneous media, e.g., [33–36]. There are also specific physical examples of non-Fourier behaviors related to Stefan phase change problems [37–39]. Direct simulations of the solidification of a phase change material (PCM), placed as a fractal pattern within a non-phase change matrix (mold), indicates that the advance of the solidification front has a super-diffusive time exponent $> \frac{1}{2}$ [37]. In contrast, direct simulations of the solidification front advance in a PCM containing non-phase change inserts, arranged as a fractal pattern, is

sub-diffusive, with a time exponent $< \frac{1}{2}$ [37]. Further, simulations of a water infiltration into a porous media [38], a limit case Stefan problem, exhibit sub-diffusive behavior in the presence of a fractal obstacle field; simulation predictions that have been experimentally confirmed [39].

Many of the works on modeling and analysis of non-Fourier Stefan problems cited above, including works from the current authors, simply start by arbitrarily replacing the first order gradient and/or time derivative in the governing equations of the classic Stefan problem with fractional derivatives of order $0 < \alpha, \beta \leq 1$. While this may lead to mathematically well posed problems, there is no guarantee that the modified governing equations obtained, in this 'ad-hoc' manner, are physically sound, i.e., it may not be possible to associate them with an appropriate thermodynamic (heat) balance that specifically identifies the mechanism for the non-Fourier heat transport. As a case in point, consider formulations of the Stefan condition. In the classic model, see [8], this condition expresses the heat balance on the moving melt interface, relating the speed of this interface to the jump in the value of the Fourier flux at the interface. In developing Stefan model formulations that account for memory two alternatives for the Stefan condition have been proposed. The first, see [15, 20], relates a fractional $0 < \alpha < 1$ rate of change of the interfaces position to the jump in the Fourier flux. In contrast, the second, see [17, 24], relates the rate of change of the interfaces position to the jump in a *memory flux*—defined as the fractional time derivative $0 < \alpha < 1$ of the Fourier flux. While, in solving one-dimensional problems, both of these alternatives produce the expected sub-diffusive time scaling, $\frac{\alpha}{2} < \frac{1}{2}$, analysis shows that the solution of the temperature fields differ [19, 24]. In particular, formulations that use a fractional rate in time for the front position [15, 20]—in keeping with the classic problem—induce a jump in the temperature gradient at the melt interface, whereas in formulations that use a memory flux the temperature gradient is continuous [25]. This dramatic difference is cause for concern, reinforced by the analysis in Voller at al [17], who argue that the two proposed interface balances provide fundamentally different treatments on how the memory associated with the melting phase change is encoded. In this light,

we feel that there is a need go beyond non-Fourier Stefan formulations that simply replace integer derivatives with fractional ones, moving towards more consistent treatments that start from a thermodynamic balance statement based on a physically reasoned accounting of memory effects.

In this work, restricting attention to melting problems at thermal equilibrium and controlled by heat conduction, our objective is to derive non-Fourier Stefan formulations from thermodynamic balance statements. We will start by writing down the heat balance for an arbitrary control volume undergoing a general melting phase change. Then use physical reasoning to arrive at a more general statement, explicitly accounting for memory in the system. From this starting point, we develop a general fractional derivative based governing equation for non-Fourier phase change systems. We argue that, an appropriate limit case of this general formulation, recovers a thermodynamically consistent and general formulation for non-Fourier Stefan melting problems, i.e., problems that exhibit—or approach—a sharp interface separating the melt from the solid. We show, supported by appropriate numerical simulations, that this sharp interface formulation implies that the Fourier flux (the gradient of temperature) is at least piecewise continuous at the phase interface and that its derivative, on the liquid side of the interface, is infinite. Findings that run counter to what is seen in the classic Stefan models, where the flux is discontinuous and its liquid side derivative is identically zero. Indeed, in the classic Stefan problem, an interface flux discontinuity is required to drive the phase change forward—the Stefan condition.

# 2 Preliminaries

To start our exploration of non-Fourier Stefan problems we need to provide, some background on general analysis approaches for Stefan problems, furnish key definitions and constructs of the fractional calculus, and identify appropriate variables and constitutive models for a melting phase change system.

## 2.1 Analysis approaches for Stefan problems

The central difficulty in solving the Stefan problem is the tracking of the sharp moving melting front defined by the isotherm $u_m$. This difficulty is compounded by the fact that, in order to accumulate the latent heat to melt the solid, the conductive heat flux needs to exhibit a jump discontinuity on the melt front. In the study of Stefan problems, the way around this issue, is to introduce a so-called 'mushy region' in which both the liquid and solid phases coexist. In the melting/solidification of alloy metal systems [1, 5–7] such regions are natural, a consequence of the alloy phase diagram. In mathematical and engineering studies of sharp interface Stefan problems, however, the mushy-region is an 'artificial' regularization device, introducing sufficient smoothness into the problem to allow for analysis [9–13] or numerical solution [2–4]. A typical approach, adopted here, is to model the mushy region as a thin temperature range around the melting isotherm, $[u_m - \epsilon, u_m + \epsilon]$, across which, the liquid fraction changes continuously and smoothly, from a value of $f = 0$ (full solid) to a value of $f = 1$ (full liquid). By physical considerations it can be readily concluded that, if the phase change is continuous and smooth, the conductive heat flux and temperature will also be continuous and smooth. The idea behind such a regularization, is that, by considering the case where the mushy region collapses to the sharp interface ($\epsilon \to 0$), results and methods arising from the mushy region approximation can be applied to the classic sharp Stefan problem. We will use this approach in the current work. Initially developing non-Fourier formulations and treatments of melting problems with a mushy-region and then considering the nature of these results as we pass to the limit of $\epsilon \to 0$.

## 2.2 Key definitions and properties of fractional calculus

Given a general function in space and time, $g(\boldsymbol{x}, t)$, the Riemann-Liouville (RL) fractional time integral of order $0 < \alpha \leq 1$ [27], is defined as,

$$ {}_{t_0}I_t^{\alpha}\, g(\boldsymbol{x}, t) = \frac{1}{\Gamma(\alpha)} \int_{t_0}^{t} (t - \tau)^{\alpha - 1} g(\boldsymbol{x}, \tau)\, \partial\tau, \tag{1} $$

where $t_0$ is a fixed initial point in time and $\Gamma(\cdot)$ is the gamma function. This definition, arising from a non-integer generalization of the Cauchy repeated integral formula, is in the form of a convolution integral; expressing how the function $(t-\tau)^{\alpha-1}$ modifies the function $g(\boldsymbol{x},t)$ over the time interval $[t_0,t]$. A physically interpretation, is a weighting of the function $g(\boldsymbol{x},t)$ back to the time origin $t_0$, with larger weights attributed to the more current times.

For later use, we note the following properties of the RL integral.

(i) By direct integration we see that the fractional integral $0<\alpha\leq 1$ of a constant $C$ is

$$ {}_{t_0}I_t^{\alpha}\, C = \frac{1}{\Gamma(\alpha)}\int_{t_0}^{t}(t-\tau)^{\alpha-1}C\,\partial\tau = C\frac{(t-t_0)^{\alpha}}{\alpha\Gamma(\alpha)}, \tag{2}$$

(ii) It immediately follows from eq.(2) that the

$$ \lim_{t\to t_0} {}_{t_0}I_t^{\alpha}\, C = 0. \tag{3}$$

(iii) For two arbitrary orders $\alpha,\beta>0$, Riemann-Liouville fractional integrals satisfy the semi-group property (see 1.3 in [27])

$$ [{}_{t_0}I_t^{\alpha}][{}_{t_0}I_t^{\beta}]g(\boldsymbol{x},t) = [{}_{t_0}I_t^{\beta}][{}_{t_0}I_t^{\alpha}]g(\boldsymbol{x},t) = {}_{t_0}I_t^{\alpha+\beta}g(\boldsymbol{x},t). \tag{4}$$

From the definition of the Riemann-Liouville integral we can define the Riemann-Liouville (RL) fractional time derivative of order $0<\alpha<1$ as

$$ {}^{RL}_{t_0}D_t^{\alpha}\, g(\boldsymbol{x},t) = \frac{\partial}{\partial t}\left[{}_{t_0}I_t^{1-\alpha}\, g(\boldsymbol{x},t)\right] = \frac{1}{\Gamma(1-\alpha)}\frac{\partial}{\partial t}\int_{t_0}^{t}(t-\tau)^{-\alpha}g(\boldsymbol{x},\tau)\,\partial\tau, \tag{5}$$

essentially stating that the Riemann-Liouville fractional derivative of order $0<\alpha<1$ is formed by the time derivative of the fractional $0<1-\alpha<1$ integral [27]. Note that [27]:

(i) The RL derivative of order $\alpha$ is the left inverse of the RL integral of order $\alpha$ ,

$$ {}^{RL}_{t_0}D_t^{\alpha}\,{}_{t_0}I_t^{\alpha}g(\boldsymbol{x},t) = g(\boldsymbol{x},t). \tag{6}$$

(ii) The RL fraction derivative of a constant is not zero ,

$$ {}^{RL}_{t_0}D_t^{\alpha}\, C = \frac{(t-t_0)^{-\alpha}}{\Gamma(1-\alpha)}C \tag{7}$$

## 2.3 Variables and constitutive models

In developing various Stefan problem models we will consider an arbitrary control volume $\Omega$, with surface $\Gamma$ and outward pointing normal $\boldsymbol{n}$, contained in a domain, with prescribed boundary conditions, undergoing a time-dependent melting process, from a solid to liquid phase, around a scaled melting temperature of $u_m = 0$.

Constitute laws for heat transfer in our control volume will be developed in terms of the Fourier heat conduction law, defining the heat flux $\left[\frac{\text{J}}{\text{m}^2-\text{s}}\right]$ as

$$\boldsymbol{q}(\boldsymbol{x}, t) = -k\nabla u(\boldsymbol{x}, t) \tag{8}$$

where $k$ $\left[\frac{\text{J}}{\text{m-s-K}}\right]$ is the thermal heat conductivity. In considering Fourier models will use this law as is. In non-Fourier memory treatments, however, we will form the constitutive equation for heat flux at a point in space as a time convolution of the Fourier heat flux at that point.

At time $t$, we will measure the heat content at a space point $\boldsymbol{x}$ in our volume with the volumetric enthalpy function $\left[\frac{\text{J}}{\text{m}^3}\right]$ defined as [8],

$$H(\boldsymbol{x}, t) = \rho c\ u(\boldsymbol{x}, t) + f(u)\rho l, \tag{9}$$

where $\rho$ $\left[\frac{\text{kg}}{\text{m}^3}\right]$ and $c$ $\left[\frac{\text{J}}{\text{kg-K}}\right]$ are the density and specific heat receptively (assumed constant), $u(\boldsymbol{x}, t)$[K] is the temperature, $l$ $\left[\frac{\text{J}}{\text{kg}}\right] \geq 0$ is the latent heat associated with melting, and $f(u)$ is the liquid fraction. To regularize the problem, we will assume that the liquid fraction is modeled by the continuous and smooth function

$$f(u) = \begin{cases} 0, & -\epsilon \geq u \\ 0.5 \sin\left(u\frac{\pi}{2\epsilon}\right) + 0.5, & -\epsilon < u < \epsilon \\ 1, & u \geq \epsilon \end{cases}; \tag{10}$$

with $\epsilon > 0$ [K] is defined as the half-temperature mushy region width. We stress that the choice of this liquid fraction function is arbitrary, any function that changes smoothly between 0 and 1, across a given temperature range, will suffice. Schematic plots of enthalpy $H(x, t)$ and liquid fraction $f$ against temperature, for various choices of latent heat $l$ and

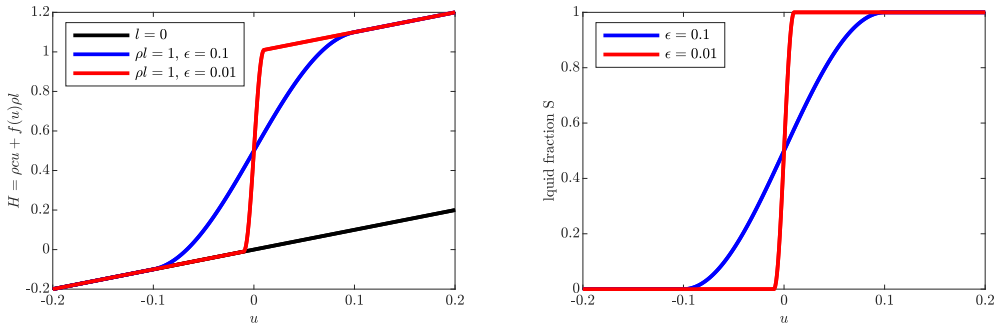


Figure 1: Schematic plots of enthalpy and liquid fraction vs. temperature.

temperature half-width $\epsilon$, are illustrated in Fig. 1. If $l = 0$ there is no phase change and the enthalpy is directly related to the temperature ($u = \frac{H}{\rho c}$). With a finite value of latent heat and a relatively large value of $\epsilon$, the effect of the increase in latent heat due the melting phase change is spread over a 'mushy region' that increases in liquid fraction with increasing temperature. When the value of $\epsilon$ becomes smaller, the phase change becomes much sharper, with a rapid change in the liquid fraction, from values close to zero, just below the temperature $u = 0$, to values very close to unity just above. In fact, by decreasing $\epsilon$ further, while still retaining a strictly positive value, we can approximate, to arbitrary accuracy, the sharp phase change at the temperature $u(\boldsymbol{x}, t) = 0$ associated with the classical Stefan problem.

# 3 Heat balance statements

## 3.1 The Fourier balance

In a conventional heat transfer setting, the appropriate heat balance equates the heat in our control volume, at time $t$, to the total heat fluxed across its surface through the time interval $[0, t]$. On defining the initial enthalpy in the control volume as $H(\boldsymbol{x}, 0)$, this balance

can be expressed as,

$$\int_\Omega \left(H(\boldsymbol{x},t) - H(\boldsymbol{x},0)\right)\ dV = -\int_0^t \int_\Gamma \boldsymbol{q}(\boldsymbol{x},\tau)\cdot \boldsymbol{n}\, dS\ dt. \tag{11}$$

By taking time derivatives of both sides we can also express this balance as

$$\frac{d}{dt}\int_\Omega H(\boldsymbol{x},t)\ dV = -\int_\Gamma \boldsymbol{q}(\boldsymbol{x},t)\cdot \boldsymbol{n}\, dS, \tag{12}$$

saying that the rate of the increase of the heat in the volume $\Omega$ is equal to the heat flux across its surface $\Gamma$.

At this point we observe that, in eq.(11) and eq.(12), the heat flux has the same weight at any time value $\tau \in (0,t)$. Implying that the system has a 'perfect memory', where the heat transfer events at all previous times are weighted equally. By contrast, in this work, we would like to explore situations where this memory weighting might change through space and time.

## 3.2 A general non-Fourier balance accounting for memory effects

For example, heterogeneities in the system ( e.g., a fractal distribution of low conductivity inclusions), might weight recent heat transfer events more heavily, slowly forgetting previous events as they recede into the past. In essence, such a behavior disrupts the perfect memory found in the balance of eq.(11), by given our system a selective memory with the ability to forget. On recalling its convolution property, we can build a model with this attribute by replacing the time integral in eq.(11) with a Riemann-Liouville fractional integral [eq.(1)]

$$\int_\Omega \left(H(\boldsymbol{x},t) - H(\boldsymbol{x},0)\right)\ dV = -{}_0I_t^\alpha \left(\int_\Gamma \boldsymbol{q}(\boldsymbol{x},t)\cdot \boldsymbol{n}\, dS\right), \tag{13}$$

where a decreasing value of the value $0 < \alpha \leq 1$ indicates a higher tendency to 'forget' past events and ${}_0I_t^\alpha(\int_\Gamma q(\boldsymbol{x},t)\cdot \boldsymbol{n}\ dS) = \frac{1}{\Gamma(\alpha)}\int_0^t(\int_G q(\boldsymbol{x},\tau)\cdot \boldsymbol{n}\ dS)(t-\tau)^{\alpha-1}d\tau$.

We can further generalize the memory model by applying the fractional integral operator ${}_0I_t^{1-\beta}$, $\alpha \leq \beta \leq 1$ to both sides of eq.(13) to get

$${}_0I_t^{1-\beta}\int_\Omega \left(H(\boldsymbol{x},t) - H(\boldsymbol{x},0)\right)\ dV = -{}_0I_t^{1+\alpha-\beta} \left(\int_\Gamma \boldsymbol{q}(\boldsymbol{x},t)\cdot \boldsymbol{n}\, dS\right), \tag{14}$$

essentially distributing the memory effect between a transient and flux term. In this generalization, the parameter $\alpha \in (0, 1]$, referred as the *memory parameter*, controls the memory in the system; indicating an increasing memory effect as $\alpha$ deceases in value. While, the parameter $\beta \in [\alpha, 1]$, referred to as *memory distribution*, controls the distribution of the memory effect between flux ($\beta = 1$) and enthalpy ($\beta = \alpha$) convolutions.

Since the enthalpy and flux are smooth and continuous, we can swap the order of integration in eq.(14) to rewrite the balance as

$$\int_\Omega {}_0I_t^{1-\beta} \left(H(\boldsymbol{x}, t) - H(\boldsymbol{x}, 0)\right)\, dV = -\int_\Gamma {}_0I_t^{1+\alpha-\beta} \boldsymbol{q}(\boldsymbol{x}, t) \cdot \boldsymbol{n}\, dS, \tag{15}$$

or, differentiating in time, and taking the time derivative inside the surface integral, as

$$\frac{d}{dt}\int_\Omega {}_0I_t^{1-\beta} \left(H(\boldsymbol{x}, t) - H(\boldsymbol{x}, 0)\right)\, dV = -\int_\Gamma \frac{\partial}{\partial t}{}_0I_t^{1+\alpha-\beta} \boldsymbol{q}(\boldsymbol{x}, t) \cdot \boldsymbol{n}\, dS. \tag{16}$$

To move forward from this statement, we propose the following generalized constitutive relationships, which when $\epsilon > 0$, will be continuous and smooth,

— the *memory enthalpy*

$$H^m = {}_0I_t^{1-\beta} \left(H(\boldsymbol{x}, t) - H(\boldsymbol{x}, 0)\right), \tag{17}$$

representing a weighted average of the heat content back through time and, using the definition of the Riemann-Liouville fractional derivative [eq.(5)] ,

— the *memory flux*

$$\boldsymbol{q}^m(\boldsymbol{x}, t) = \frac{\partial}{\partial t}{}_0I_t^{1+\alpha-\beta} \boldsymbol{q}(\boldsymbol{x}, t) = {}^{RL}_0D_t^{\beta-\alpha} \boldsymbol{q}(\boldsymbol{x}, t), \tag{18}$$

physically interpreted as the time derivative of a decreasing weighted sum of the Fourier flux at position $\boldsymbol{x}$ back through time.

These relationships allow us to write the balance in eq.(16) in the more compact form,

$$\frac{d}{dt}\int_\Omega H^m(\boldsymbol{x}, t)\, dV = -\int_\Gamma \boldsymbol{q}^m(\boldsymbol{x}, t) \cdot \boldsymbol{n}\, dS, \tag{19}$$

referred to as the *memory balance*. Pay particular attention to the fact that this balance is identical in form to the more standard balance in eq.(12). Equation (19) still equates

the rate of heating in the volume to the flux across its surface but now with generalized enthalpy and flux constitutive relationships that, through appropriate time convolutions, account for memory effects. Note, if we set $\alpha = 1$ then $\beta = 1$, and we recover the standard form [eq.(12)] from eq.(19).

# 4 Governing domain equation

Let us now consider a one dimensional problem in the domain, $x \in [0, L], L >> 1, t \in [0, T]$. Initially the domain contains solid and a constant temperature $u(x, 0) = u_{in} \leq 0$. At time $t > 0$ the temperature at $x = 0$ is raised and fixed to the temperature $u_0 > 0$ — initiating a phase change—while the temperature at $x = L$ remains fixed at the initial value $u(L, t) = u_{in}$. Considering an arbitrary fixed section $[a, b]$ of our domain, we can write the general balance in eq.(19) as

$$\frac{d}{dt}\int_a^b H^m dx = -q^m(b, t) + q^m(a, t) \tag{20}$$

On noting that, (i) $a$ and $b$ are fixed points, (ii) $H^m$ is continuous and differentiable, (iii)

$$\int_a^b q_x^m(x, t)dx = q^m(b, t) - q^m(a, t), \tag{21}$$

and, (iv) by the Reynold Transport theorem,

$$\frac{d}{dt}\int_a^b H^m dx = \int_a^b \frac{\partial H^m}{\partial t} dx, \tag{22}$$

we can rewrite eq.(20) as

$$\int_a^b \frac{\partial H^m}{\partial t} + q_x^m(x, t)\ dx = 0 \tag{23}$$

Or, since the interval $[a, b]$ is arbitrary chosen from $[0, L]$,

$$\frac{\partial H^m}{\partial t} + q_x^m(x, t) = 0, \quad 0 < x < L. \tag{24}$$

Further, (i) through the definitions of the memory enthalpy in eq.(17) and the Riemann-Liouville fractional derivative in eq.(5), we see that

$$\frac{\partial H^m}{\partial t} = {}^{RL}_{0}D_t^{\beta}(H(x, t) - H(x, 0)) \tag{25}$$

and (ii) through the definitions of the memory flux in eq.(18) and Fourier flux $q = -ku_x(x,t)$, we see that

$$q_x^m(x,t) = -\frac{\partial}{\partial x}\left(k\ {}^{RL}_{0}D_t^{\beta-\alpha}u_x(x,t)\right) \tag{26}$$

With these relationships in hand we can expand eq.(24) as

$${}^{RL}_{0}D_t^{\beta}(H(x,t) - H(x,0)) - \frac{\partial}{\partial x}\left(k\ {}^{RL}_{0}D_t^{\beta-\alpha}u_x(x,t)\right) = 0, \quad 0 < x < L, \tag{27}$$

where $0 < \alpha \leq 1,\ \alpha \leq \beta \leq 1$. This is our proposal for a *general mushy melting phase change model formulation*, accounting for memory effects by setting a value $\alpha \in (0,1)$ and distributing these effects between a memory enthalpy and flux by setting the value of $\beta \in [\alpha, 1]$.

We make three observations related to the general model formulation in eq.(27):

- The value of of the memory parameter $0 < \alpha \leq 1$ determines the 'level' of memory in the system. In a given application, we would expect each value of $\alpha$ to provide a unique solution.

- The value of distribution $\beta$ determines the orders of the fractional derivatives in the memory enthalpy and memory flux terms. Since eq.(27) was derived from the general balance statement in eq.(14) —by the inverse property of the RL derivative eq.(6)—it is reasonable to expect that, for a given value of $\alpha$, any arbitrary choice of $\beta$ in the range $[\alpha, 1]$ will, result in equivalent formulations.

- If we set $\alpha = 1$ ( implying that $\beta = 1$) in eq.(27), we recover the standard and well known enthalpy formulation, see [8],

$$\frac{\partial}{\partial t}H(x,t) - \frac{\partial}{\partial x}\left(ku_x(x,t)\right) = 0. \quad 0 < x < L, \tag{28}$$

  Like this basic form, the more general memory form in eq.(27) is valid throughout the domain $[0, L]$. Further, in a similar fashion to the basic enthalpy method, we can apply eq.(27) to approximate the sharp interface problem by simply choosing a very small value of $\epsilon << 1$. In fact, in practice, in seeking a numerical solution for such a case, it is convenient to set $\epsilon = 0$ in the definition of the enthalpy $H$ given in eq.(9).

# 5 Governing sharp interface equations

## 5.1 Derivation of equations

Now let us consider a case where our interval $[a, b]$ contains the isotherms $u = -\epsilon$ and $u = \epsilon$ located at positions $s^-(t)$ and $s^+(t)$ respectively. From eq.(23), this allows us to write down three balances, one over the full liquid sub-interval $[a, s^-]$,

$$\int_a^{s^-} \frac{\partial H^m}{\partial t} + q_x^m(x,t)\ dx = 0, \tag{29}$$

one over the full solid sub-interval $[s^+, b]$,

$$\int_{s^+}^{b} \frac{\partial H^m}{\partial t} + q_x^m(x,t)\ dx = 0, \tag{30}$$

and one over the mushy sub-interval $[s^-, s^+]$

$$\int_{s^-}^{s^+} \frac{\partial H^m}{\partial t} + q_x^m(x,t)\ dx = 0, \tag{31}$$

On recognizing that

$$\int_{s^-}^{s^+} q_x^m(x,t)\ dx = \left[q^m(s^+,t) - q^m(s^-,t)\right],$$

and using the Reynold transport theorem,

$$\int_{s^-}^{s^+} \frac{\partial H^m}{\partial t}\ dx = \frac{d}{dt}\int_{s^-}^{s^+} H^m(x,t)\ dx\ + \left[-\frac{ds^+}{dt}H^m(s^+,t) + \frac{ds^-}{dt}H^m(s^-,t)\right],$$

we can rewrite the balance in eq.(31), over the sub interval $[s^-, s^+]$, as

$$\frac{d}{dt}\int_{s^-}^{s^+} H^m(x,t)\ dx + \left[-\frac{ds^+}{dt}H^m(s^+,t) + \frac{ds^-}{dt}H^m(s^-,t)\right] + \left[q^m(s^+,t) - q^m(s^-,t)\right] = 0 \tag{32}$$

As we pass to the limit of a sharp phase change, i.e., $\epsilon \to 0$, (i) the $\epsilon$ and $-\epsilon$ isotherms approach the melt isotherm $u = 0$, at position $s(t)$, i.e., $s^- \to s^+ \to s$ , (ii) the integral $\int_{s^-}^{s^+} H^m(x,t)\ dx \to 0$, and (iii) the velocities of the $\epsilon$ and $-\epsilon$ isotherms approach the velocity of the melt front, i.e., $\frac{ds^-}{dt} \to \frac{ds^+}{dt} \to \frac{ds}{dt}$. In this way, on recalling the arbitrary choice of the

fixed points $a$ and $b$, we can derive the following sharp interface governing equations from eqs.(29) and (30),

$$\frac{\partial H^m}{\partial t} + q_x^m(x,t) = 0, \quad 0 < x < s(t), \quad 0 < t < T \tag{33a}$$

$$\frac{\partial H^m}{\partial t} + q_x^m(x,t) = 0 \quad s(t) < x < L, \quad 0 < t < T. \tag{33b}$$

The initial condition is $u(x,0) = u_{in}$, eq.(33a) has boundary conditions $u(0,t) = u_0$ and $u(s,t) = 0$, whereas the boundary conditions for eq.(33b) are $u(s,t) = 0$ and $u(L,t) = u_{in}$. Both equations are subject to an additional condition on the melt front, a generalized Stefan condition, obtained from the $\epsilon \to 0$ limit case of eq.(32),

$$[\![ H^m ]\!]_-^+ \frac{ds}{dt} - [\![ \, q^m ]\!]_-^+ = 0, \quad 0 < t < T, \tag{34}$$

where $[\![]\!]$ represents the jump from the liquid to the solid side of the melt interface $s$.

## 5.2 Interface flux conditions

A core result form our above analysis, is that, for a specified value of the memory parameter $\alpha$, any choice of the distribution parameter $\beta$, in the range $[\alpha, 1]$, results in an equivalent model formulation. Thus, in exploring properties of the sharp interface model defined in eq.(33) and eq.(34) we can, with no loss in generality, consider the special case of $\beta = \alpha$. That is the case where $q^m = q = -ku_x(x,t)$, the Fourier flux, and

$$H^m = {}_0I_t^{(1-\alpha)} \left[ \rho c u(x,t) - \rho c u_{in} + \rho l f(u) \right], \tag{35}$$

where we note for a sharp interface, the liquid fraction $f(u)$, see eq.(10), is a Heaviside step function.

Our interest here is to investigate the nature of the Fourier heat flux $q = -ku_x$ and its derivative $q_x = -ku_{xx}$ at the melt interface. We know that, in the classical Stefan problem, the flux exhibits a jump discontinuity at the interface and its derivative, on the liquid side, is zero [8]. Will we recover similar conditions when we have memory, $0 < \alpha < 1$?

From eq.(35) we see that at points $x$ on the solid side of the melt interface ($u < 0$), where melting has not commenced, the liquid fraction $f(u) = 0$ throughout the time interval $[0, t]$ and we can write the solid memory enthalpy as

$$H_s^m = {}_0I_t^{(1-\alpha)} \left[\rho c u(x,t) - \rho c u_{in}\right] \tag{36}$$

On the other hand, for points $x$ on the liquid side, the liquid fraction takes a value of $f(u) = 0$ over the time interval $[0, h(x))$ and a value of $f(u) = 1$ over the time interval $[h(x), t]$, where $h(x)$ is the time that the melt front arrives at position $x$. Thus, on the liquid side of the melt interface,

$$H_l^m = {}_0I_t^{(1-\alpha)} \left[\rho c u(x,t) - \rho c u_{in}\right] + {}_{h(x)}I_t^{(1-\alpha)}[\rho l] \tag{37}$$

Since the first term on the left matches the memory enthalpy in the solid we can write down the jump in memory enthalpy across the interface as

$$[\![H^m]\!]_l^s = \lim_{t \searrow h(\boldsymbol{x})} {}_{h(\boldsymbol{x})}I_t^{1-\alpha} \left[\rho l\right], \tag{38}$$

There is an important and interesting observation to be drawn from this result. From our listed properties of the RL fractional integral [eq.(1)] we know that, when the value of $\alpha$ is strictly in the interval $(0, 1)$ the fractional integral of the constant value $\rho l$, ${}_{h(\boldsymbol{x})}I_t^{1-\alpha}\left[\rho l\right]$, will vanish as $t \to h(\boldsymbol{x})$. This implies that, when $\alpha < 1$, the memory enthalpy has no jump across the melt interface, rather it is continuous, i.e., $[\![H^m]\!]_l^s = 0$. In turn, through the Stefan condition in eq.(34), there is no jump in the Fourier flux across the melt interface, i.e.,

$$[\![\ -k u_x(x,t)]\!]_l^s = 0 \tag{39}$$

Note, however, when there are no memory effects, i.e., $\alpha = 1$, the integral operator on the left of eq.(38) becomes the identity operator and the jump in enthalpy takes the value of $\rho l$, matching, as we should expect, the jump in the classical Stefan condition [8],

$$-[\![\ k u_x(x,t)]\!]_l^s = \rho l \frac{ds}{dt}. \tag{40}$$

On first glance the result in eq.(39) appears to be in direct conflict with the classical integer Stefan problem where the flux discontinuity across the interface is required to provide the heat to melt and advance the phase change process. This dramatic contrast with the classical case could be a cause for concern for the physical validly of the non-Fourier treatments presented here. However, on closer inspection, we see that this result is a natural consequence of the regularization induced by defining the heat content as the memory-enthalpy ${}_0I_t^{1-\alpha}(H(x,t) - H(x,0))$. With this step, the phase change—the accumulation of sufficient latent heat to complete melting—does not occur instantaneously but rather smoothly over time. Thus, the memory enthalpy can be viewed as a regularization for the classic sharp interface model, a regularization that offers an alternative to the more conventional approach of introducing a mushy region phase change, as in eq.(9).

In addition, we note that, continuity of flux at the melt interface has been seen in previous studies of memory Stefan problems. In one-phase memory Stefan problems, where the initial condition is solid at the phase change temperature $u(x,0) = 0$, the continuity of flux at the melt interface will manifest as a zero flux value $ku_x(x,t) = 0$ on the liquid side of the interface. Kubica and Ryszewska [25] note this zero flux condition in their mathematical analysis of the one-dimensional one phase Stefan memory-flux formulation. Further, a specific closed solution for a limit case memory-enthalpy model, developed in [19], exhibits a zero flux at the melt interface.

We get an equally interesting result in considering the derivative of the flux $q_x = -ku_{xx}$ on the liquid side of the interface. Retaining the case where $\beta = \alpha$ and using the memory enthalpy definition in eq. (35), the governing equation in eq (33), on the liquid side of the sharp interface, can be written as

$$ {}^{RL}_{0}D_t^{\alpha}\left[\rho c u(x,t) - \rho c u_{in}\right] + {}^{RL}_{h(x)}D_t^{\alpha}[\rho l], -ku_{xx}(x,t) = 0, \quad 0 \le x \le s(t). \tag{41} $$

Since $\rho$ and $l$ are constants we can directly evaluate the second fractional derivative

$$ {}^{RL}_{0}D_t^{\alpha}\left[\rho c u(x,t) - \rho c u_{in}\right] + \rho l \frac{(t-h(x))^{-\alpha}}{\Gamma(1-\alpha)} - ku_{xx}(x,t) = 0 \tag{42} $$

or multiplying through by $(t-h(x))^{\alpha}$

$$(t-h(x))^{\alpha}\left({}^{RL}_{0}D^{\alpha}_{t}\left[\rho c u(x,t)-\rho c u_{in}\right]\right)+\frac{\rho l}{\Gamma(1-\alpha)}-k(t-h(x))^{\alpha}u_{xx}(x,t)=0 \qquad (43)$$

Due to the smoothness of the temperature, we can expect the fractional derivative of $(u-u_{in})$ to be bounded throughout the liquid phase. Thus, when $\alpha<1$, as we approach the melt interface, i.e., as $(t-h(x))^{\alpha}\to 0$, the first term will vanish and the only way to maintain the equation is for the derivative of the flux on the liquid side of the interface $u_{xx}(x,t)\to\infty$. Which, once again, is in conflict with the expected behavior for the classic case ($\alpha=1$) where the derivative of the flux vanishes at the melt interface.

## 5.3 Numerical verification of interface flux conduction

We can provide numerical calculations that support our findings related to the flux and its derivative at the melt interface. For this we continue to consider, without loss of any generality, the case where $\beta=\alpha$. We will, however make one additional simplification, setting the initial value in the domain to $u_{in}=0$. This reduces our problem to a one domain melting problem, where heat transfer only occurs in the melt, the solid phase ($x>s(t)$) remaining at the constant melt temperature $u_m=0$, throughout the calculation. Thus, based on our analysis here, when $\alpha<1$, we would expect to see that the liquid side flux, at the melt interface takes a value of zero while its derivative is infinite.

We will numerically solve the full domain formulation, eq.(27) with $\beta=\alpha$, which on noting the one-phase nature of the problem and that fact that the initial enthalpy $H(x,0)=0$, can be written as

$${}^{RL}_{0}D^{\alpha}_{t}H(x,t)-ku_{xx}(x,t)=0,\quad t>0,\quad 0\le x<L, \qquad (44)$$

In making this solution we will assume that the temperature width of the mushy region is very small $\epsilon<<1$.

To numerically solve eq.(44) we use the time implicit unconditionally stable scheme presented in detail by Voller [19]. As detailed in the Appendix, we make some small

changes to this scheme related to the approximation of the fractional derivatives and the use of a direct solver.

We consider the problem where $u_0 = \rho = k = c = l = 1$. The solution uses a finite difference grid with 105 nodes points, equally spaced at a distance $\Delta x = 0.01$. We will consider two cases, the classic non-memory integer case $\alpha = 1$, employing a time step of $\Delta t = 0.001$ and a fractional case $\alpha = 0.5$, employing a time step of $\Delta t = 2 \times 10^{-5}$. In both cases we will continue to solve the problem until the front is located at position $s = 1$. Following [40, 41], we assume that the melt front is located at node $i$ ($s = i\Delta x$) when the nodal liquid fraction $f_i = 0.5$. Thus, we can estimate the time $t_i$ to reach a particular node $i$, by linearly interpolating between the times $t = j\Delta t$ and $t = (j + 1)\Delta t$ whenever $f_i^{j+1} > 0.5$ and $f_i^j < 0.5$.

As a verification, Fig. 2 show numerical predictions for the advance of the interface ($s = i\Delta x$), plotted as $\log(i\Delta x)$ vs. $\log t_i$, $i = 1, 2, \ldots$. The $\alpha = 1$ predictions are extremely well fit by the power-law $s = 1.24t^{0.5}$, which is the exact analytical solution of this case [8]. The $\alpha = 0.5$ predictions are also fit by a power-law but now with an exponent of 0.25, i.e., $s = 1.3766t^{0.25}$, recovering the expected sub-diffusion scaling of $n = \alpha/2$. Recalling that time $t_{100}$ is the numerical estimate for the melt front to arrive at position $s = 100\Delta x = 1$, we made this later fit by assuming the form $s = at^{0.25}$, determining the value of the pre-factor as $a = t_{100}^{-0.25}$.

Figure 3 shows the predicted nodal temperature profiles ($\alpha = 1, 0.5$). In panel a. these are plotted as $u$ vs. $x$. Note, that the integer case ($\alpha = 1$) has very little curvature as we approach the melt interface $s = x = 1$. A behavior that is consistent with the expected interface jump in the temperature gradient dictated by the Stefan condition. However, when $\alpha = 0.5$, there is a distinct concaved up curvature in the temperature profile, suggesting the possibility that the temperature gradient may approach a value of zero at the melt interface. We can provide a more quantitative argument by considering the plot of $\log(u_i)$ vs. $\log(1 - x_i)$, $i = 1, 2 \ldots 99$ shown in panel b. of Fig. 3. Note, how, for both the integer and fractional case, in the vicinity of the melt interface, the temperature profile asymptotes

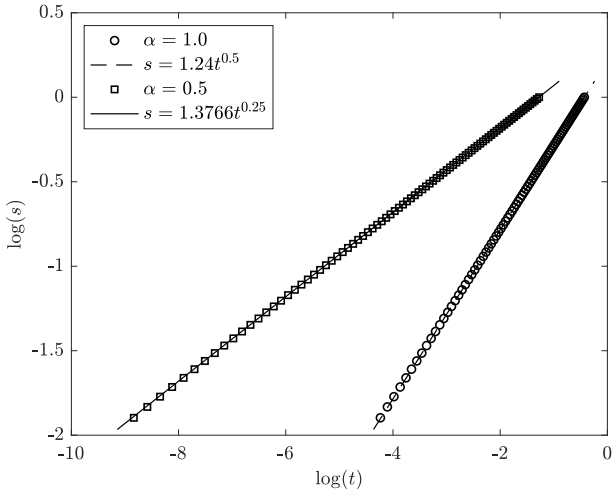


Figure 2: Predictions for the movement of the melt interface, $\log(s)$ vs. $\log(t)$.

to a power-law $u \sim (1 - \frac{x}{s})^n$, obtained by the linear fit between $(\log(1 - x_{98}), \log(u_{98}))$ and $(\log(1 - (x_{99}), \log(u_{99}))$. When $\alpha = 1$, a fit for this power-law exhibits, to three places, the exponent $n = 1.000$. Thus we see that the flux, (the temperature gradient) at the interface takes the time dependent value $-ku_x \sim \frac{1}{s}$ and its derivative $-ku_{xx} = 0$. These are the results we expect for the classic case, e.g., when we use the interface flux in the Stefan condition [eq.(40)] the melt front moves as the square root of time $s \sim t^{\frac{1}{2}}$. On the other hand, when we consider the fractional case $\alpha = 0.5$, the fit exponent of the power-law is $n = 1.452$. Indicating that, as we approach the interface $x \to s$, the flux $-ku_x \sim -(1 - \frac{x}{s})^{0.452} \to 0$ and its derivative $-ku_{xx} \sim -(1 - \frac{x}{s})^{-.548} \to \infty$; recovering our theoretical result. Note, as an indication that we have reached reasonable grid convergence in the results presented above, if we repeat the calculation with the coarser step $\Delta x = 0.02$ we get a fit exponent, when $\alpha = 0.5$, of $n = 1.455$.

## 5.4 Physical realization of sub-diffusive behavior

As a validation of our the theory presented here, we provide a physical realization of the sub-diffusive evolution of a melting phase change. For this, building on previous experiments and direct simulations [37–39], we consider a domain with a two-dimensional $(x, y)$ square

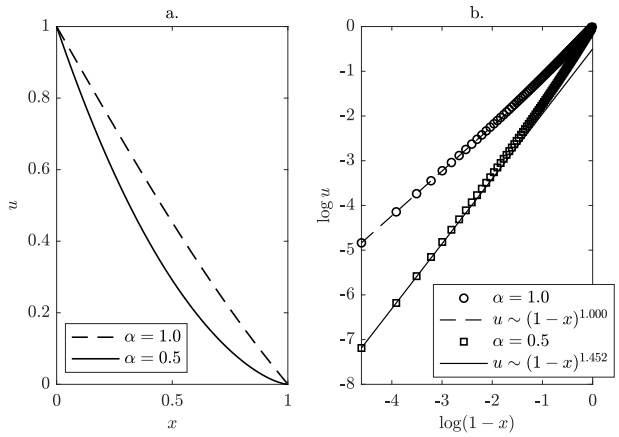


Figure 3: Predictions of the temperature profile when the melt front is on $s = 1$. (a) $u(x)$ vs. $x$. (b) $\log u$ vs. $log(1 - x)$. Note, with reference to (b) how, in the vicinity of the melt interface $x = s = 1$, the profiles asymptote to power-laws of the form $(1 - \frac{x}{s})^n,\ n \geq 1$.

planform of size $128 \times 128$ and a nominal thickness of $\Delta z = 1$, The domain contains a fractal (3rd order Sierpinski carpet) distribution of through thickness ceramic inserts, see Fig. 4, with unit values of specific heat and density ($c = 1, \rho = 1$) and a very low conductivity value of $k = 10^{-6}$. The spaces between the inserts contains a solid phase change material (PCM) with a latent heat value of $l = 1$ and unit values for specific heat, density and conductivity ($c = 1, \rho = 1$, k=1). Initially, the PCM and the inserts are at a temperature $u = 0$, the melting temperature of the PCM. At time $t = 0$, the left vertical face of the domain, along $x = 0$, is raised and fixed at the temperature of $u = 1$. Thus, as time advances, the PCM material will begin to melt and heat up, while, due to their low conductivity, the inserts will remain close to the initial temperature ($u = 0$). Following [37], we can model this 2D melting process, through a direct simulation, using a standard enthalpy formulation

$$\frac{\partial H}{\partial t} = \nabla \cdot (k \nabla u). \tag{45}$$

Note in the inserts, where $k << 1$ we can approximate $\partial H/\partial t \approx 0$ and in PCM regions the enthalpy $H = cu + f$ (recall $0 \leq f \leq 1$) is the liquid fraction. For future reference, we also note that, in the limit case of specific heat $c \to 0$, the governing equation becomes

$\partial f/\partial t = \nabla\cdot(k\nabla u)$; on replacing temperature $u$ with pressure $p$ and conductivity $k$ with the Hele-Shaw permeability, this governing equation and the associated boundary conditions, exactly match the governing equation for fluid infiltration into a Hele-Shaw cell containing obstacles laid out as a Sierpinski carpet (see eq. (1) in [38]). Thus we can view this infiltration problem as a physical limit case of our proposed PCM melting problem.

The enthalpy formulation in eq.(45) can be readily solved with an explicit in time control volume scheme. operating on a grid of $(128 \times 128)$ square control volumes with sides $\Delta x = \Delta y = 1$. At any point in time, in this direct simulation, we predict a nodal liquid fraction field, where in the inserts and unmelted regions $f = 0$, in the melted regions $f = 1$, and in the melting regions $0 < f < 1$; Fig. 4 indicates the melted region, at the point where melting has advanced up to the 2nd order of the Sierpinski carpet. Note, the advance of the melting trends strongly in the $x-$direction and we can characterize the advance, in this direction, by tracking the effective melting length

$$s(t) = \frac{\sum_{i=1}^{128}\sum_{j=1}^{128} f_{i,j}}{128} \tag{46}$$

where $f_{i,j}$ are the predicted nodal liquid fractions at time $t$. Figure 5, shows, as a log-log plot, the advance of the effective length with time. This plot clearly indicates that the advance of the effective melting length is power-law in time, i.e., $s(t) \sim t^n$. Moreover, fitting shows that the time exponent is sub-diffusive, $n = 0.3588 < 0.5$.

There are two important points to make in regard to this direct melting simulation:

1. Previous research [39], experientially investigated infiltration into Hele-Shaw cells containing obstacles laid out as a Sierpinski carpet. Which, as we have noted above, is a limit case of our proposed physical realization. In this light, it is noteworthy that the sub-diffusive time exponent obtained from these experiments ($n = 0.3463 \pm 0.018$, see Fig. 6 in [39]), is an excellent match for the exponents ($n = 0.3588$) obtained from our direct melting simulation; providing an experimental validation.

2. Predictions based on our proposed continuum theory will readily recover any sub-diffusive scaling seen in experiments or direct simulations through simply setting the

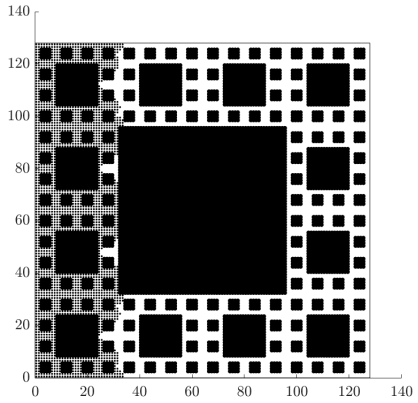


Figure 4: Melting in a Sierpinski carpet, heated on the left side, insulated on all other sides. The dark squares, the carpet elements, are inserts with a very low relative conductivity ($k = 10^{-6}$). Surrounding the inserts is a phase change material (PCM). The lighter shading represents the melting of the PCM at the point where melting extends to the 2nd order element.

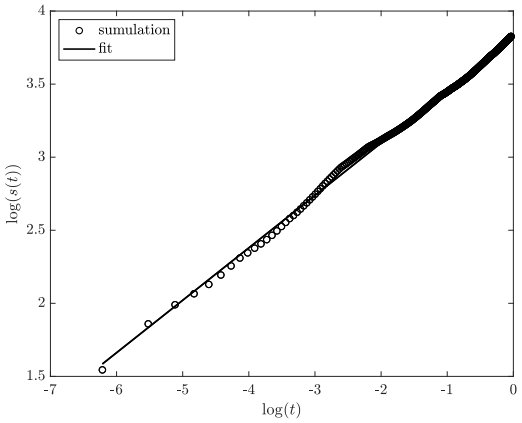


Figure 5: Log-log plot of the advance of the effective melting length, eq.(46), follows a power-law with a sub-diffusive exponent $n = 0.3588$.

appropriate values of the parameters $\alpha$ and $\beta$. For example setting $\alpha = 2 \times 0.3588$ in solving the memory enthalpy formulation in eq.(44).

# 6 Discussion and Conclusion

In deriving models that describe heat conduction controlled heat transport, the obvious starting point is to first define constitutive relationships for heat content (e.g., an enthalpy) and heat flux (e.g., the Fourier heat conduction). Quantities that can be used to form a heat balance, equating the rate of change of enthalpy in a control volume to the rate that heat is fluxed in across the volumes surface. From this thermodynamic statement, through appropriate mathematical operations, governing equations, in terms of partial time and space derivatives can then be derived.

The question we are answering in this work is how to establish fractional derivative models of anomalous heat transfer systems that can be directly related to thermodynamic heat balance statements. Our focus has been on the development of models for Stefan melting problems, employing fractional time derivatives to account for memory effects. To arrive at these models, we have proposed generalized constitutive relationships, for what we refer to as a memory enthalpy [eq.(17)] and a memory flux [eq.(18)]; formed as time convolutions of the enthalpy and Fourier flux respectively. With the memory enthalpy and flux we are able to form a thermodynamic balance, the memory balance [eq. (19)], mimicking the standard heat balance form, through equating the rate of change of the memory enthalpy in a control volume with the memory flux crossing its surface. Key features in this balance, are the ability to control the memory in the system through setting a parameter $\alpha \in (0, 1)$ (a value of $\alpha = 1$ indicating no memory effects) and the ability to control the distribution of the memory effect between the memory enthalpy and flux, by setting a parameter $\beta \in [\alpha, 1]$.

From our proposed memory balance, we have developed a general fractional derivative model formulation for melting phase change problems [eq.(27)]—or by simple extension, any solid-liquid heat conduction controlled phase change. This model formulation assumes that

the phase change (the accumulation of latent heat) occurs smoothy across a temperature range $[-\epsilon, \epsilon]$. This formulation can be directed at the Stefan melting problem, exhibiting a sharp moving melt interfaces, by (i) choosing an arbitrarily small value of $\epsilon << 1$, or (ii) by reposing the formulation in the limit of vanishing $\epsilon$, to arrive at an equivalent sharp interface model [eqs. (33) and (34)]. Both formulations retaining the generality of setting values for the memory $\alpha \in (0, 1)$ and distribution $\beta \in [\alpha, 1]$ parameters.

We emphasis the fact that all of the memory Stefan model formulations obtained in this work are directly and consistently related to the common thermodynamic balance statement in eq.(19). Thus, we feel that it is reasonable to make the conjecture that they are equivalent. That is, a thermal field that satisfies a particular formulation will be a solution for any other model, derived from eq.(19), that has the same value of $\alpha$. This is an important attribute, because an analysis result or approximate numerical solution, made for one model formulation, will be universal. We have made use of this feature in the current work. The numerical scheme presented in the Appendix can be the basis for developing an approximate solution for any model formulation consistently derived from the memory balance [eq.(19)]. Also, the analysis of the flux conditions at the interface, made around model formulations with $\beta = \alpha$, readily show how use of fractional calculus introduces a regularization that leads to a continuous flux at at the melt interface. A feature that we can conclude, is present in any other model formulation based on the memory balance in eq.(19), regardless of the value of distribution parameter $\beta$.

The point we would most like to emphasize in our work is the need to be thermodynamically consistent in developing fractional calculus models for heat transfer applications in particular and reactive transport models in general. We hope we have made the case that the utility and understanding of these models is significantly enhanced if they can be directly related to a thermodynamic balance statement. A statement that explicitly identifies and includes the physical mechanism(s) that induce anomalous transport behaviors.

# Appendix: Implicit time numerical solution

Our objective is to numerically solve the eq. (44) on a finite difference grid of $n+1$ equally spaced ($\Delta x$) node points ($i = 0, 1 \ldots, n, n+1$), using a constant time step of $\Delta t$. We will assume fixed temperatures for the end nodes ($u_0 = 1, u_{n+1} = 0$), solving for the unknowns at nodes $1, 2, \ldots, n$. In making the discretization of eq.(44) we will approximate the Riemann-Liouville fractional derivative of the enthalpy at time level $j+1$, $t = (j+1)\Delta t$ using Grünwald weights (generalized repeated backward differencing) of the time derivative [42]

$$ {}_0^{RL}D_t^{\alpha} H\big|_i^{j+1} \approx \Delta t^{-\alpha} \sum_{p=0}^{j+1} g_p H_i^{j+1-p} \tag{47} $$

where the weights

$$ g_0 = 1, \quad g_p = g_{p-1}\left[\frac{p-1-\alpha}{p}\right], \; p = 1, 2 \ldots . \tag{48} $$

With this approximation, using a central difference approximation for the divergence of the temperature gradient, we arrive at the following time implict scheme for eq.(44),

$$ H_i^{j+1} = -\sum_{p=1}^{j+1} g_p H_i^{j+1-p} + k\frac{\Delta t^{\alpha}}{\Delta x^2}(u_{i-1}^{j+1} - 2u_i^{j+1} + u_{i+1}^{j+1}), \quad j = 0, 1, 2 \ldots; 1 \le i \le n. \tag{49} $$

Noting, here, that the initial temperature is $u_{in} = 0$ we can write

$$ H_i^{j+1} = \rho c u_i^{j+1} + f_i^{j+1} l, \tag{50} $$

arriving at the non-linear system for solving the temperature nodal field at time level $j+1$

$$ \mathbf{A}\mathbf{u}^{j+1} = \mathbf{b} \tag{51} $$

In this system, on row $i = 1, 2, \ldots n$ of $\mathbf{A}$

$$ a_{i,i-1} = k\frac{\Delta t^{\alpha}}{\Delta x^2}, \quad a_{i,i} = -\rho c - 2k\frac{\Delta t^{\alpha}}{\Delta x^2}, \quad a_{i,i-1} = k\frac{\Delta t^{\alpha}}{\Delta x^2} \tag{52} $$

with all other coefficients set at zero and

$$ b_1 = \sum_{p=1}^{j+1} g_p H_i^{j+1-p} + f_i^{j+1} l - k\frac{\Delta t^{\alpha}}{\Delta x^2}, \quad b_i = \sum_{p=1}^{j+1} g_p H_i^{j+1-p} + f_i^{j+1} l, \;\; i = 2, 3, \ldots n \tag{53} $$

The system is non-linear since both the current $(j+1)$ temperature and liquid fraction node fields are unknown.

In solving this non-linear system we will set the mushy temperature range $\epsilon = 0$ (the sharp interfaces limit). In this limit, through inversion of eq.(10), we see that when $0 < f_i^{j+1} < 1$ the corresponding nodal temperature will be $u_i^{j+1} = 0$. Further, at any point in the solution there will only be one node in the domain ($w$ say) where the phase change is occurring, i.e., only one node where $0 < f_w^{j+1} < 1$. Thus we can extend the well known liquid fraction update enthalpy scheme [4] to solve eq.(51).

Let us assume that at time level $j$ the phase change is occurring around node $w$. Then, in solving for time level $j+1$:

- We set the coefficient $a^*_{w,w} = 10^{10}$, a sufficiently large value.
- Solution of eq.(51), using a packaged sparse matrix solver, will then predict a value of $u_w^{j+1} = 0$.
- In this case, if the phase change at time level $j+1$ is still around node $w$ we can assume the predicted nodal temperature field is correct.
- With this temperature field we can then update the liquid faction at node $w$ as

$$f_w^{j+1} = \frac{-\sum_{p=1}^{j+1} g_p H_w^{j+1-p} + k\frac{\Delta t^\alpha}{\Delta x^2} u_{w-1}^{j+1}}{l} \tag{54}$$

  note the temperature values at $w$ and $w+1$ have been forced to values of zero by the setting of $a^*_{w,w}$.
- If the predicted value of the liquid fraction, at node $w$, remains within $(0,1)$, i..e, $f_w^{j+1} \in (0,1)$, the solution for the current temperature and liquid fraction nodal fields will be correct and complete and we can move calculation to the next time step.
- Otherwise, if $f_w^{j+1} > 1$, indicating that the phase change is completed at node $w$, we (i) set $f_w^{j+1} = 1$, (ii) reset $a_{w,w} = -\rho c - 2k\frac{\Delta t^\alpha}{\Delta x^2}$, (iii) increment the phase change node $w = w+1$ and, (iv) repeat the solution process.

We typically arrive at a converged solution for the current temperature and liquid fraction nodal fields within one iteration, only in cases where the phase shifts from one node to the next will additional iterations be needed. Hence solution is very efficient.

## Acknowledgments

Vaughan Voller's research supported as part of the Center on Geo-processes in Mineral Carbon Storage, an Energy Frontier Research Center funded by the U.S. Department of Energy (DOE), Office of Science, Basic Energy Sciences (BES), under Award No. DE-SC0023429 (theoretical developments of fractional calculus models of reactive transport systems). In addition, Vaughan Voller acknowledges support of the James L Record professorship, Department of Civil, Environmental, and Geo- Engineering, University of Minnesota and Sabrina Roscani acknowledges support from Austral No. 006-INV00030 (Rosario, Argentina).

## References

[1] N.R. Eyres, D.R. Hartree, J. Ingham, R.J. Sarjant and J.B. Wagstaff, The calculation of variable heat flow in solids, Philosophical Transactions of the Royal Society, Series A, Mathematical and Physical Sciences, 240(813) (1946), pp.1–57.

[2] G. Comini, S. Del Guidice, R.W. Lewis, and O.C. Zienkiewicz, Finite element solution of non-linear heat conduction problems with special reference to phase change. Int. J. Numer. Meth. Engng., 8 (1974), pp. 613–624.

[3] K. Morgan, R.W. Lewis, and O.C. Zienkiewicz, An improved algorithm for heat conduction problems with phase change, Int. J. Numer. Meth. Engng., 12 (1978), pp. 1191–1195.

[4] V.R. Voller, C.R. Swaminathan, and B.G. Thomas, Fixed grid techniques for phase change problems: A review., Int. J. Numer. Meth. Engng., 30 (1990), pp. 875–898.

[5] W.D. Bennon and F. P. Incropera, A continuum model for momentum, heat and species transport in binary solid-liquid phase change systems—I. Model formulation, International Journal of Heat and Mass Transfer 30(10) (1987), pp. 2161–2170.

[6] C. Beckermann and R. Viskanta, Double-diffusive convection during dendritic solidification of a binary mixture, PhysicoChemical Hydrodynamics 10(2) (1988), pp. 195–213.

[7] V. R. Voller, A. D. Brent, and C. Prakash, The modelling of heat, mass and solute transport in solidification systems, International Journal of Heat and Mass Transfer 32(9) (1989), pp. 1719–1731.

[8] J. Crank, Free and moving boundary problems, Clarendon Press, Oxford, 1984.

[9] A.A. Lacey, J.R. Ockendon, and A.B. Tayler, Modelling mushy regions, in Lecture Notes in Control and Information Sciences N.44, Springer Verlag, Berlin (1982), pp.111–126.

[10] M. Primicerio, and M. Ughi, Phase-change problems with mushy regions, in Free Boundary Problems: Application and Theory. Vol. 120. Pitman Research Notes in Mathematics, 1985.

[11] H.M. Yin, Regularity of the interfaces in the Stefan problem with a mushy region, Canad.Math.Bull., 35 (1992), pp.136-144

[12] M. Bertsch, N.H.A Klaver The Stefan problem with mushy regions: Differentiability of the interfaces, Ann.Mat.Pura Appl., 166 (1994), pp.27–61.

[13] A.D. Solomon, D.G. Wilson, and V. Alexiades, A mushy zone model with an exact solution. Letters in Heat and Mass Transfer, 9(4) (1982), pp. 319–324.

[14] B. Šarler, Stefan's work on solid-liquid phase changes, Engineering Analysis with Boundary Elements 16(2) (1995), pp. 83–92.

[15] J. Liu, M. Xu, Some exact solutions to Stefan problems with fractional differential equations, J. Math. Anal. Apps., 351 (2009), pp. 536–542.

[16] V.R. Voller, An exact solution of a limit case Stefan problem governed by a fractional diffusion equation, International Journal of Heat and Mass Transfer 53 (23-24) (2010), pp. 5622–5625.

[17] V.R. Voller, F Falcini, R Garra, Fractional Stefan problems exhibiting lumped and distributed latent-heat memory effects, Phys. Rev. E., 87 (2013), 042401.

[18] M.S. Kushwaha, Homotopy perturbation method for a limit case Stefan problem governed by fractional diffusion equation, Applied Mathematical Modelling 37(5) (2013), pp. 3589–3599.

[19] V.R. Voller, Fractional Stefan problems, Int. J. Heat Mass Trans., 74 (2014), pp. 269–277.

[20] M. Błasik, and K. Małgorzata, Numerical solution of the one phase 1D fractional Stefan problem using the front fixing method, Mathematical Methods in the Applied Sciences 38(15) (2015), pp. 3214–3228.

[21] X.Gao, X. Jiang, and S. Chen, The numerical method for the moving boundary problem with space-fractional derivative in drug release devices, Applied Mathematical Modelling 39(8) (2015), pp. 2385–2391.

[22] S. Roscani, J. Bollati, D. A. Tarzia, A new mathematical formulation for a phase change problem with a memory flux, Chaos Solitons and Fractals, (116) (2018), pp. 340–347.

[23] S.D. Roscani, D.A. Tarzia, Two different fractional Stefan problems that are convergent to the same classical Stefan problem, Math Meth Appl Sci., 41 (2018), pp. 6842–6850.

[24] S. Roscani, N. Caruso and D. Tarzia, Explicit solutions to fractional Stefan-like problems for Caputo and Riemann–Liouville derivatives, Communications in Nonlinear Science and Numerical Simulation, 90 (2020), 105361.

[25] A. Kubica, K. Ryszewska, A self-similar solution to time-fractional Stefan problem, Math Meth Appl Sci., 44 (6) (2021), 4245–4275.

[26] S. G. Samko, A. A. Kilbas, and O. I. Marichev, Fractional Integrals and Derivatives: Theory and Applications. Gordon and Breach, 1993.

[27] R. Gorenflo and F. Mainardi, Fractional Calculus, Fractals and fractional calculus in continuum mechanics, Springer, 1997, pp. 223–276.

[28] R. Hilfer, Applications of Fractional Calculus in Physics, Word Scientific Publishing Co., Singapore, 2000.

[29] Y. Povstenko, Linear Fractional Diffusion-Wave Equation for Scientists and Engineers, Springer, San Diego, 2015.

[30] B. Baeumer, M. Kovács, M. Meerschaert, H. Sankaranarayanan, Boundary conditions for fractional diffusio. Journal of Computational and Applied Mathematics 336 (2018), pp. 408–424.

[31] F. Falcini, R. Garra, V. R. Voller, Modeling anomalous heat diffusion: Comparing fractional derivative and non-linear diffusivity treatments, Int. J. Therm. Sci., 137 (2019), pp. 584–588.

[32] V.R, Voller, Anomalous heat transfer: Examples, fundamentals, and fractional calculus models, Advances in Heat Transfer, 50 (2018), pp. 333–380.

[33] H. Ahmadikia and A. Moradi, Non-Fourier phase change heat transfer in biological tissues during solidification. Heat Mass Transfer 48 (2012), pp.1559–1568.

[34] B. Yu, X. Jiang, and C, Wang, Numerical algorithms to estimate relaxation parameters and Caputo fractional derivative for a fractional thermal wave model in spherical composite medium, Applied Mathematics and Computation 274 (2016), pp.106–118.

[35] D. Kumar and K. N. Rai, Numerical simulation of time fractional dual-phase-lag model of heat transfer within skin tissue during thermal therapy, Journal of Thermal Biology 67 (2017), pp. 49–58

[36] X. Wang, H.Qi, X.Yang, and H.Xu, Analysis of the time-space fractional bioheat transfer equation for biological tissues during laser irradiation, International Journal of Heat and Mass Transfer 177 (2021), 121555.

[37] V.R. Voller, Computations of anomalous phase change, International Journal of Numerical Methods for Heat and Fluid Flow 26(3-4) (2016), pp. 624–638.

[38] V.R. Voller, A direct simulation demonstrating the role of spacial heterogeneity in determining anomalous diffusive transport, Water Resources Research 51(4) (2015), pp. 2119–2127.

[39] N. Filipovitch, K.M. Hill, A. Longjas, and V.R. Voller, Infiltration experiments demonstrate an explicit connection between heterogeneity and anomalous diffusion behavior, Water Resources Research, 52 (7) (2016), pp. 5167–5178.

[40] P.H. Price, and M.R. Slack, The effect of latent heat on numerical solutions of the heat flow equation, British Journal of Applied Physics, 5(8) (1954), pp. 285–287.

[41] V. R. Voller, and M. Cross, Accurate solutions of moving boundary problems using the enthalpy method, International Journal of Heat and Mass Transfer 24 (3) (1981), pp. 545–556.

[42] R. Schumer, M. M. Meerschaert, and B. Baeumer, Fractional advection-dispersion equations for modeling transport at the Earth surface, Journal of Geophysical Research: Earth Surface 114 (F4) (2009).